IBMS BoneKEy. 2008 November;5(11):410-425
http://www.bonekey-ibms.org/cgi/content/full/ibmske;5/11/410
doi: 10.1138/20080348

PERSPECTIVES

CT-Based Visualization and Quantification of Bone Microstructure *In Vivo*

G. Harry van Lenthe[1,2] and Ralph Müller[2]

[1]Division of Biomechanics and Engineering Design, K.U.Leuven, Leuven, Belgium
[2]Institute for Biomechanics, ETH Zürich, Zürich, Switzerland

Abstract

It is well-accepted that in addition to bone volume, trabecular bone microstructure is an important factor influencing bone strength, which in turn is the most important bone parameter indicating bone fracture risk. The objective of this article is to describe some of the computed tomography (CT)-based techniques used to measure the microarchitectural aspects of bone quality, how these can be quantified and how these quantitative endpoints can be used in the assessment of bone competence. Microarchitectural bone imaging is a nondestructive, noninvasive, and precise procedure with which both the apparent density and trabecular microstructure of intact bones and bone samples can be assessed in a single measurement. Recently introduced high-resolution *in vivo* CT imaging systems now allow repetitive measurements of bone microarchitecture so that small local trabecular changes can be monitored over time. The procedure can help improve predictions of fracture risk, clarify the pathophysiology of skeletal diseases, and define the response to therapy and interventions. Hopefully, this improved understanding will lead to more successful approaches in the prevention and treatment of age- and disease-related fractures. *IBMS BoneKEy*. 2008 November;5(11):410-425.

Introduction

Osteoporosis is not a disease of low bone mass *per se*, but of low bone strength. The present "gold standard" to determine bone strength is through mechanical testing. Direct mechanical testing is a straightforward procedure, but is limited by its destructiveness. Therefore, this method is not applicable *in vivo*, and although it can be used *in vitro*, a sample can only be tested once, which limits the assessment of direction-dependent failure characteristics. Furthermore, these tests are prone to errors related to boundary artifacts and to the often small size of the specimens, hampering high precision measurements (1).

Bone mineral density (BMD) measurements are frequently used as a surrogate measure of bone strength. Significant correlations between the apparent bone density and different mechanical properties have been demonstrated for large populations using power-law regressions (2;3). A meta-analysis showed that for trabecular bone samples, around 64% of the variability in bone strength *in vitro* is determined by its apparent density (4). Bone microstructure explains a significant part of the remaining variation; by including architectural parameters in the analysis the predictive power increases to over 90% for bone stiffness (5-7). Given that bone stiffness and strength are highly correlated (R^2 > 0:95; (8;9)) the effects of bone microarchitecture are very likely to strongly affect bone strength as well. Indeed, this was shown by recent experimental data that used strength as an outcome parameter and which demonstrated the significant contribution of bone architecture in predicting bone strength (10). Also, for whole bone strength, bone microarchitecture plays a significant role. In a study (11) on the dose-dependent effect of ibandronate treatment on bone mass and architecture in ovariectomized (OVX) monkeys, it was found that bone mineral content (BMC) as assessed by dual-energy X-ray absorptiometry was the best single

predictor of whole bone strength (r^2 = 67%); by including architectural indices in a multiple linear regression analysis the correlation increased to 88%.

The introduction of microstructural imaging systems such as desktop micro-computed tomography (μCT) has made it possible to assess both the apparent density and the three-dimensional (3D) trabecular microstructure of intact bones in a single measurement. It has given researchers a powerful tool for the exploration of age-related bone loss and metabolic diseases such as osteoporosis. In this *Perspective* we will present methodologies to quantify bone microstructure, to measure bone deformation under load and to assess bone competence *in silico*. The focus will be on recently introduced *in vivo* systems that allow us to image and quantify bone microarchitecture in small animals and at peripheral sites in humans.

Three-Dimensional Imaging of Bone Microarchitecture

Computed tomography is an approach used to image and quantify trabecular bone in 3D, providing multi-scale biological imaging capabilities with isotropic resolutions ranging from a few millimeter (clinical CT), to few tens of micrometers (μCT) down to one hundred nanometer (synchrotron radiation nanoCT). An overview of the principles and methodologies is beyond the scope of this paper and can be found elsewhere (12;13). μCT has become the method of choice in quantifying 3D bone microstructure. Commercially available desktop μCT systems provide nominal resolutions ranging from roughly 1 to 100 μm, allowing investigators to measure specimens with diameters ranging from a few millimeters to 100 mm. Desktop μCT is a precise and validated technique (14-16) that has been used extensively to study bone microarchitecture (16-19) and has demonstrated that trabecular bone can have very distinct microarchitectures that are remarkably heterogeneous throughout the skeleton (20-22) (Fig. 1).

Quantification of Bone Micro-Architecture

Quantitative endpoints have become an important factor for success in basic research and the development of novel therapeutic strategies in biology and biomedicine. One method of quantitatively describing bone architecture and the changes associated with age or stage of a disease is the calculation of morphometric indices, also referred to as quantitative bone morphometry. In the past, structural properties of trabecular bone have been investigated by the examination of 2D sections of bone biopsies. 3D morphometric parameters were then derived from 2D images using stereological methods (23).

In order to take full advantage of the volumetric data as obtained from μCT measurements, several new 3D image processing methods have been presented, allowing direct quantification of bone microarchitecture (21;24). These techniques calculate actual distances in 3D space and, therefore, do not rely on an assumed model type and are not biased by possible deviations.

More recently, local morphometry was introduced to measure morphometric indices of single trabecular elements, such as individual plates and rods. For this purpose, the elements have to be extracted from the structure, which can be done using a method called volumetric spatial decomposition (25). With this method it is hence possible to perform more detailed analyses of three-dimensional structures and to aid in a further understanding of the individual contribution of rods and plates to the competence of trabecular bone (26;27). As an example, in a study on human vertebral bone samples, a multiple linear regression model combining mean trabecular spacing (Tb.Sp), mean slenderness of the rods (<Ro.Sl>), and the relative amount of rod volume to total bone volume (Ro.BV/BV) was able to explain 90% of the variance in bone stiffness. This model could not be improved by adding BV/TV as an independent variable (26).

IBMS BoneKEy. 2008 November;5(11):410-425
http://www.bonekey-ibms.org/cgi/content/full/ibmske;5/11/410
doi: 10.1138/20080348

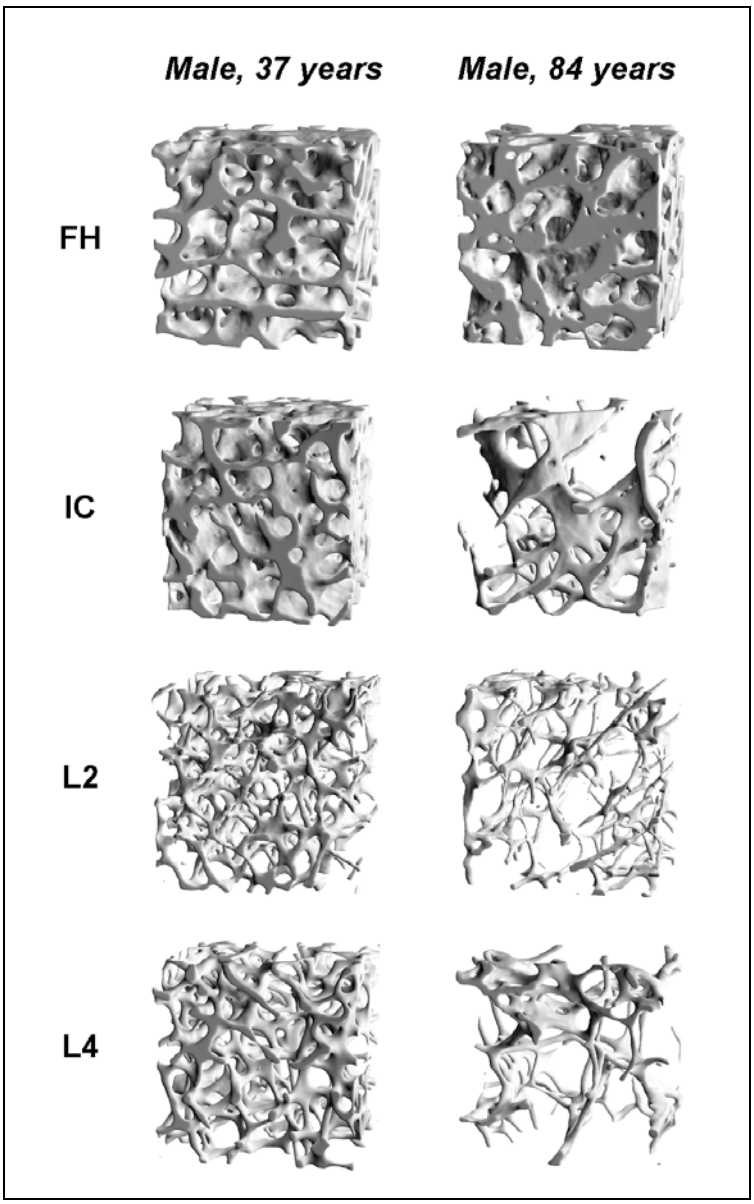

Fig. 1. Bone biopsies of a 37-year-old and an 84-year-old male taken at the femoral head (FH), iliac crest (IC), and lumbar spine (L2 and L4). Note the strong heterogeneity in bone architecture, not only between individuals but also between anatomical sites.

Visualization of Bone Under Load

Basic knowledge of local trabecular failure is still lacking. In estimating the risk of spontaneous fractures, an extended understanding of the failure behavior of trabecular bone is essential. By combining experimental testing with µCT it has become possible to visualize and quantify bone deformations under load as well as fracture initiation and progression in a non-destructive and 3D fashion (28;29). Several deformation modes were found in human vertebral bone; some trabeculae bend, others buckle, and some are compressed (30) (Fig. 2 and Suppl. Material 1). It is important to note that failure behavior might be quite different for bone in an *in vivo* environment where boundary conditions differ significantly from *in vitro* setups. For the purpose of extrapolating the findings on the material level to the *in vivo* situation in whole bones, we recently built a larger image-guided failure assessment (IGFA)

IBMS BoneKEy. 2008 November;5(11):410-425
http://www.bonekey-ibms.org/cgi/content/full/ibmske;5/11/410
doi: 10.1138/20080348

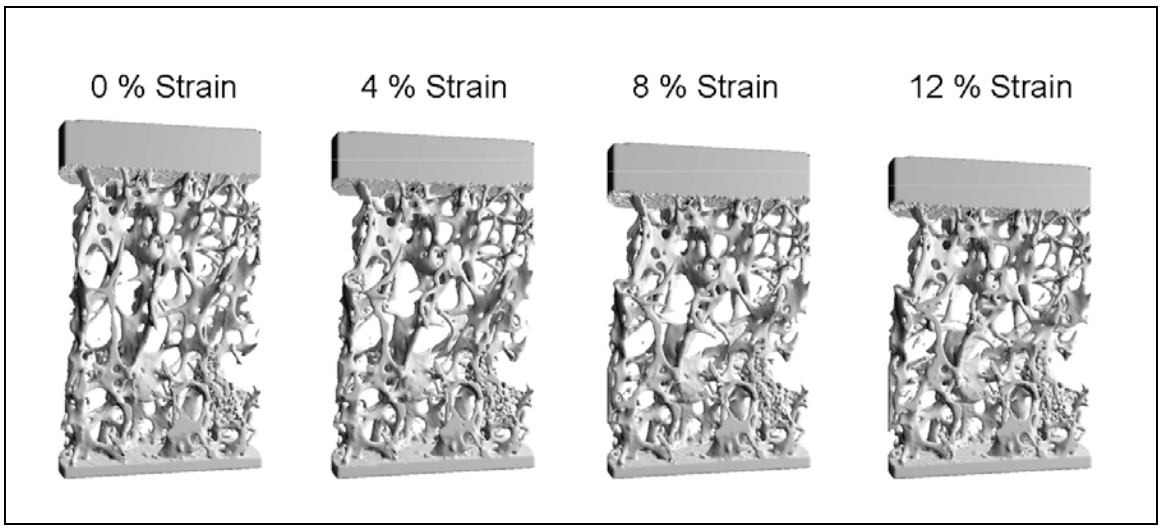

Fig. 2. Image-guided failure assessment in a human spine sample using time-lapsed tomographic imaging. The images show compression, imaged in steps of 4% strain. Note that only half of the specimen is depicted here, which is possible due to the non-invasive character of the IGFA technique (images courtesy of Dr. Martin Stauber, ETH Zürich, Switzerland).

device that can fit bones up to 10 cm in diameter. A pilot study on an ovine spinal unit clearly demonstrated its functionality in determining fracture location and progression under load (Suppl. Material 2). This technique of IGFA has been validated as compared to classical continuous mechanical testing (29;30). The deformation behavior has been quantified by determining the strains between local anatomical features (nodes) in the structure that were followed directly in the structure throughout all the steps (31). Although inter-node strains can identify loaded elements, they cannot determine the precise deformation of these elements. A better description of local strains is expected from experimental strain mapping approaches (32-34). Strain mapping is a mathematical technique to calculate how a bone or bone sample has deformed between two loading steps. For that purpose, the displacement field is calculated that maps one loading condition (*e.g.*, an undeformed object) to another loading condition (the deformed object). Based on the displacement field, the local strains can then be easily determined. As an example, deformable registration was recently implemented (34) to calculate the displacement field that mapped two images of an ovine spinal unit under compression (Fig. 3; the same experiment as illustrated in Suppl. Material 2). Based on the Gaussian filtered displacement field, the Green-Lagrange strain tensor was calculated.

Computational Assessment of Bone Competence

Although the novel experimental IGFA approaches allow new and valuable insight into the bone failure process, their application is limited to *in vitro* investigations due to their destructive nature. Computational failure prediction would therefore be a valuable tool in combination with noninvasive *in vivo* imaging to assess bone competence in living subjects. Finite element (FE) analysis is the most widely used computational technique for structural analysis in engineering. It can provide insight into the load transfer through the bone architecture and with that improves our understanding of how differences in bone microarchitecture influence bone strength. Microstructural FE (μFE) models allow researchers to perform 'virtual experiments' on computer reconstructions of trabecular bone. These models typically represent small trabecular regions in the order of 5 to 10 mm cubes, a scale at which the bone behaves as a continuum (35). As an example of such an analysis, the principal strains in a human bone biopsy subject to a compressive load are shown (Fig. 4). Loading and deformation for each

IBMS BoneKEy. 2008 November;5(11):410-425
http://www.bonekey-ibms.org/cgi/content/full/ibmske;5/11/410
doi: 10.1138/20080348

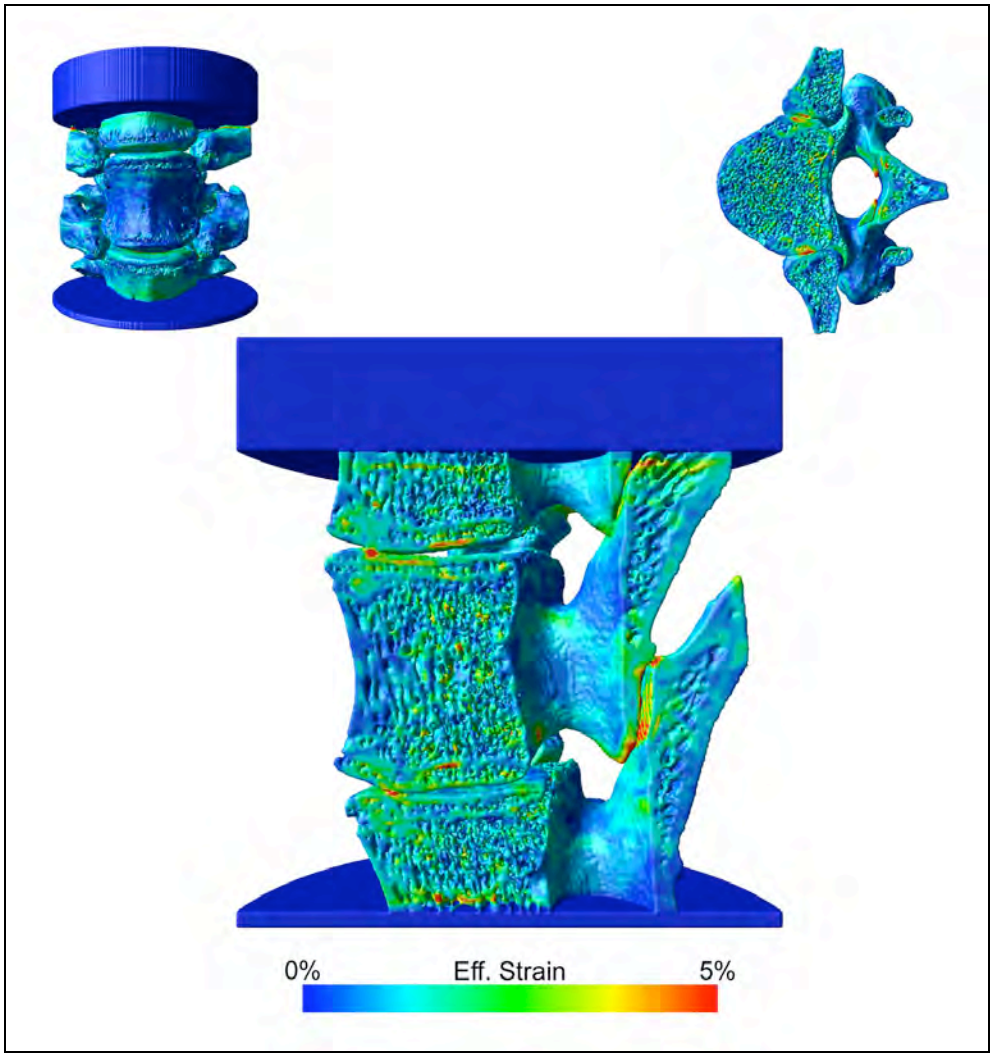

Fig. 3. Effective strains in an intact ovine spinal unit as determined from strain mapping based on two time-lapsed tomographic images (images courtesy of D. Christen, ETH Zürich, Switzerland).

individual trabecula can be determined and explored with high detail. Animation of the predicted deformations and associated stresses can help us to better understand the local failure behavior of the trabecular bone network (Suppl. Material 3).

For linear deformation conditions, comparison between biomechanical compression tests on excised trabecular bone samples and μFE show very good agreement (R^2=0.92) when a homogeneous, isotropic tissue modulus is applied (36;37); this holds true for normal as well as osteoporotic bone (38). Also for non-linear deformation conditions, good agreement was found between μFE results and experimental tests. It has been shown that at the apparent level, these μFE models can accurately predict trabecular bone failure for bovine (39) as well as for human trabecular bone (40); the μFE-predicted apparent stresses and strains at failure were equal to experimentally measured values for the same bone specimens. Whether the good agreement also holds at the level of single trabeculae and hence whether the precise location of local bone failure can be determined from μFE has yet to be determined. Nevertheless, the clinically most interesting parameter, apparent bone strength, can be accurately assessed, demonstrating that the quality of μFE analyses has reached such accuracy that they can be used as an alternative to destructive mechanical tests (39).

IBMS BoneKEy. 2008 November;5(11):410-425
http://www.bonekey-ibms.org/cgi/content/full/ibmske;5/11/410
doi: 10.1138/20080348

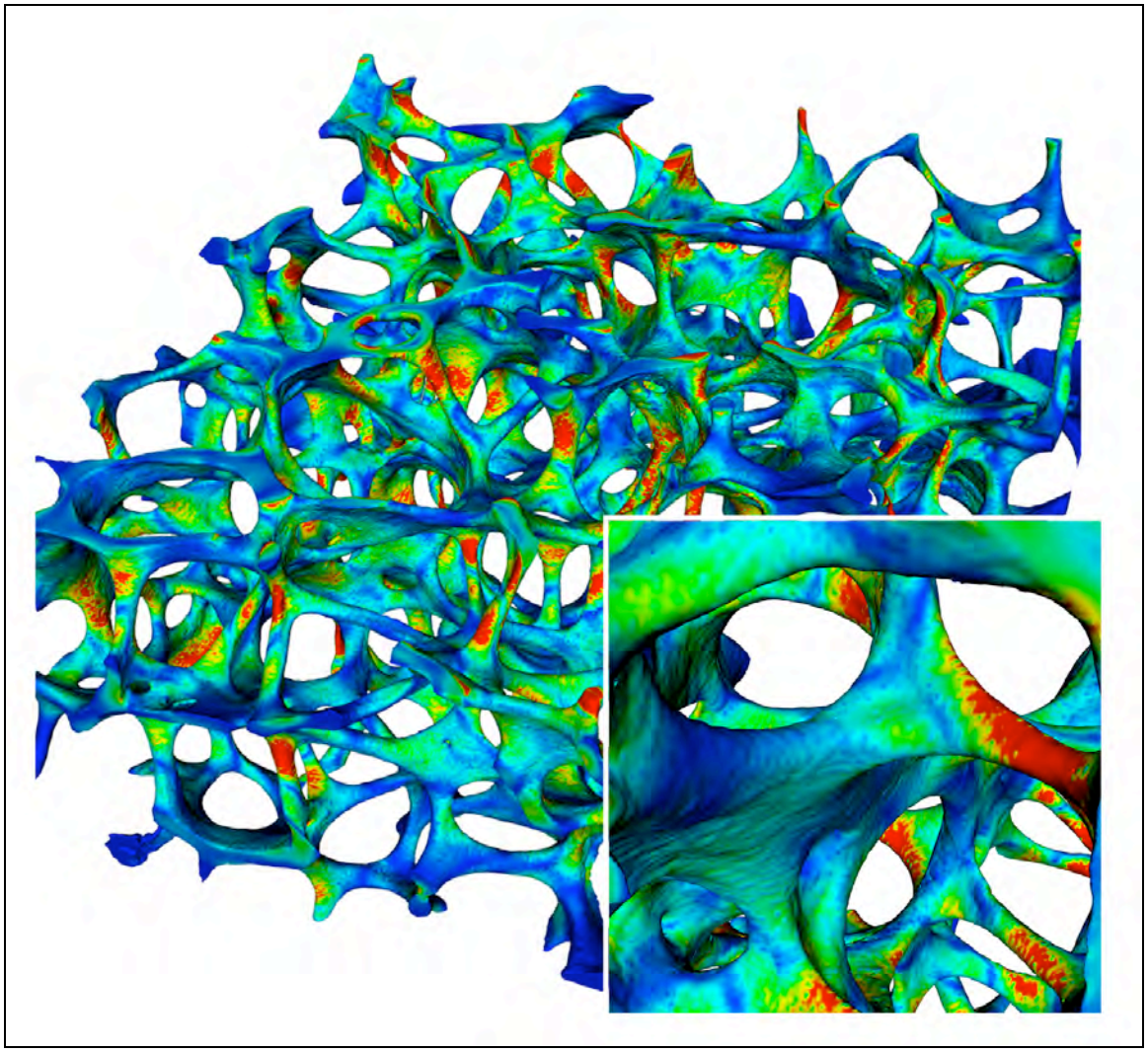

Fig. 4. Effective strains in a human iliac crest biopsy, subject to a simulated axial load, and calculated by μFE analysis. Blue: low strain; red: high strain. The inset shows part of the model in higher magnification (images courtesy of Andreas J. Wirth, ETH Zürich, Switzerland).

The steady increase in computational power over the last several years, using multiple processors in supercomputers, has made it possible to analyze intact human bones, or large portions thereof. Highly-detailed μFE models, with resolution of 60-80 μm, of the proximal human femora (41) and of human vertebra (42;43) have been presented, with up to 100 million elements. A recent implementation even allowed the solution of a model with nearly 1.5 billion degrees of freedom within 30 minutes, to simultaneously increase the level of detail and the size of the analyzed bone volume (44;45). These models have addressed aspects of osteoporosis on the stress distribution in trabecular bone, and assessed the importance of the thin cortical shell in human vertebrae. Recent μ FE analyses (element size 82 μm) on 9.1 mm thick sections at the distal radius show excellent reproducibility in stiffness and strength, with precision errors better than 1.2% CV precision for a standard analysis region (46). These models also show excellent accuracy. When using a homogeneous tissue modulus, the apparent stiffness as calculated by linear μ FE correlated highly (R^2=0.972) with experimentally assessed bone strength; the correlation could even be improved (R^2=0.983) when moduli were determined

from scaled CT-attenuation values (47). Hence, these models allow the assessment of mechanical bone properties fully non-destructively and with that the prediction of bone strength in longitudinal *in vivo* studies in a time-lapsed fashion.

Recent Developments in Small Animal *In Vivo* µCT

The feasibility of performing *in vivo* µCT was first demonstrated in the rat proximal tibia using synchrotron radiation (48), and was used to depict bone loss after OVX (49). The recent introduction of desktop µCT systems, for *in vivo* scanning of small animals (50;51), with resolution better than 10 µm has opened the way to more practical and better accessible systems. A great feature of *in vivo* scanning is that it allows for longitudinal scanning of the same animal. Hence, a time series of several images of the same bone can be obtained, which allows for the visualization and quantification of changes in bone geometry as well as changes to individual trabeculae (Fig. 5). In a way, this is similar to the time series as obtained with IGFA, but there are some important differences.

First, the time steps are in the order of weeks, such that biological adaptations causing microstructural changes can be followed over time. Hence, growth, aging, response to interventions and response to treatment can be closely monitored. Visual examinations of image-registered data show compelling evidence that small changes can be detected in the shape and orientation of single trabeculae and even parts thereof (51). However, the proper metrics to quantify these changes have yet to be introduced. Furthermore, reproducibility data for *in vivo* scanning of small animals is scarce. One study showed small errors of less than 3% in bone volume measurements and errors less than 0.5% in measurements of trabecular thickness (51). These values may differ for other types of scanners, and may also depend on the animal under investigation, its genetic background, its age, and on the specific bone location. In principle, *in vivo* reproducibility may reach that of *in vitro* studies, where excellent reproducibility has been reported for cortical (precision errors ranging from 0.06–2.16% CV) and trabecular (precision errors ranging from 0.59–5.24%) bone parameters, respectively (52).

However – and this is the second difference – radiation is a concern in *in vivo* measurement because ionizing radiation can cause damage to bone cells and impair their function and viability. Hence, a measurement can interfere with the normal bone response. Of course, this is an unwanted side effect that may limit use of *in vivo* scanning, particularly when the detrimental effects would be large compared to the effects one would like to measure, or when the architectural features that one wants to resolve are small. The latter would require a small voxel size and hence a high radiation dose, considering that a reduction in voxel size with a factor of two requires an eight-fold increase in X-ray dose to obtain the same signal-to-noise ratio. Hence, irradiation effects have received quite some attention so as to obtain the best resolution-for-dose; nevertheless, the precise effects of current *in vivo* µCT devices are still subject to some debate. It is clear that the total radiation dose depends on µCT design, scanning protocol, and the number of repeat measurements; it also seems obvious that the time interval between measurements can play a role. Furthermore, potential effects on bone structure may depend on the animals under investigation (rats or mice), be genetically influenced, and be affected by the age of the animals. In rats, Klinck *et al.* and Brouwers *et al.* detected no effects on bone structure (53;54) nor on cell viability (53) even after eight weekly scans. However, Waarsing *et al.* noticed a small effect in rats that were scanned less often (55). This could be related to several issues such as the longer follow-up, the use of a different scanning system with different dosage or the age of the animals. In mice, multiple measurements do seem to have a small effect on trabecular bone volume (~10-20% less bone relative to non-radiated limbs) (54); however, that same study also showed that effects of OVX were much larger and that there was no interaction between radiation and OVX treatment. In any case, more thorough studies seem warranted to investigate the optimal imaging

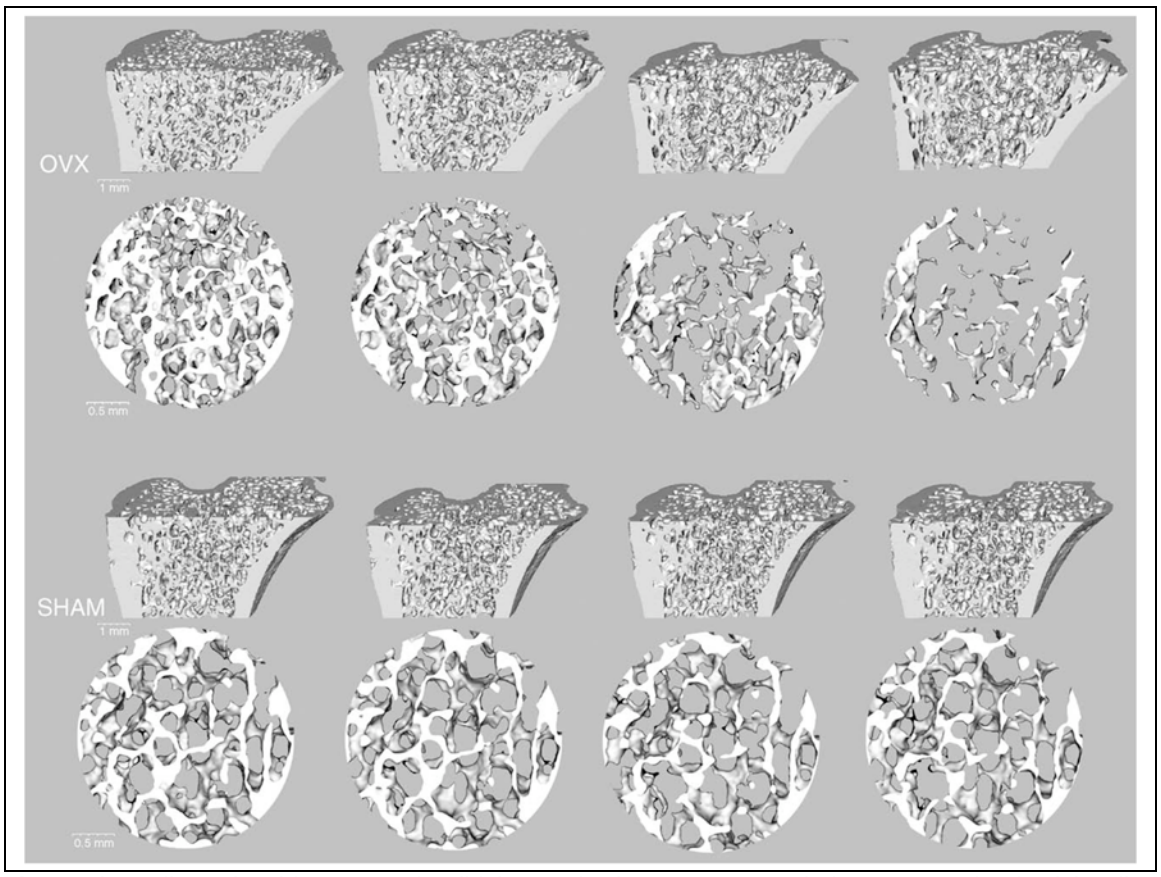

Fig. 5. Three-dimensional images of the tibial metaphysis of an OVX and sham-operated animal (median from each group) at the time of operation and follow-up measurements 1, 2 and 3 months later. The image data are transected to illustrate the internal trabecular structure, and all images were aligned using 3D image registration. Details from each time point (0.3 mm slice) are illustrated in circular cutouts (reprinted from Boyd *et al. Bone*. 2006 Oct;39(4):854-62, with permission from Elsevier).

settings providing the best resolution-for dose and the maximal number of repetitions for a given time interval.

A third difference is that *in vivo* scanning is technically more demanding: more effort is needed to match two consecutive scans. The principle of this process, called image registration, is to reorient a µCT data set such that it aligns with the data set of an earlier measurement. The differences after registration identify the locations where bone has been resorbed, and where it has been added. When changes are small, this is a relatively straightforward approach; however, it becomes a non-trivial task when architectural changes are large (51). In that case, *a priori* knowledge, *e.g.*, a fixed position of an arterial opening in the cortex, can help to identify the correct reorientation. Also, in the case of longitudinal growth, one would typically register the epiphyseal and metaphyseal bone separately to avoid mismatches due to growth by apposition at the growth plate (55). Hence, zooming in on a specific region might give a different matching then when applied on an entire bone, which implies that it is not evident how to determine the precise locations of bone loss and bone gain. Clearly, more research is needed investigating the best strategies for regional analysis in longitudinal studies where bone size and structure are changing over time in health, disease and treatment, especially in growing children or fracture healing, where large changes can be expected in a relatively short time frame.

From a methodological point of view, a great advantage of using time-lapsed *in vivo* scanning is that each animal can act as its own control, thereby increasing statistical

power. Small changes in bone structure may become detectable that would otherwise go unnoticed because of normal population variations. This was nicely demonstrated in a study on morphological changes after OVX in rats (56); the *in vivo* analysis found significant changes at an earlier time point in OVX rats and detected small changes in sham-operated rats that were not detected by the cross-sectional design. Increased statistical power also means that fewer animals are needed to detect a certain effect. Furthermore, there is no need to sacrifice animals at intermediate time points; hence, this will lead to a further reduction in the number of animals, with the reduction factor identical to the number of measurements.

Several reports have been presented on different aspects of microarchitectural changes. Using *in vivo* µCT in rats, Waarsing *et al.* observed that, due to normal aging, the combination of bone loss and bone formation resulted in alignment of trabeculae across the growth plate; this process was even more pronounced in aging OVX rats (55). Brouwers *et al.* determined the effects of the time point of bisphosphonate treatment after OVX in rats (57). The rapid bone loss and structural degradation as seen after OVX could be completely inhibited by a single injection of zoledronic acid at the time of OVX, whereas an injection eight weeks after OVX improved bone mass and structure but no full recovery was seen. The effects of genetic background on OVX-induced bone loss in mice were recently assessed by Klinck and Boyd (58). They quantified the weekly loss of bone in an animal-specific manner and found that inbred strains with higher baseline bone density values showed higher rates of bone loss.

In Vivo Scanning of Human Bone Structure

Paired iliac crest bone biopsies have been and still are being used to determine response to treatment (19;59). It is clear that these are far from ideal, first, because the procedure requires taking two invasive biopsies with associated problems, second, because the biopsies are necessarily small, and third, because in fact two different trabecular architectures are being evaluated. The drawbacks of paired biopsies could be avoided with the introduction of *in vivo* imaging systems with a resolution better than 50 µm. Unfortunately, such systems are not yet available, but the resolution at peripheral sites is approaching a level that allows elucidation of individual microstructural bone elements. Such high-resolution peripheral quantitative CT systems (HR-pQCT) have reached the market, allowing for *in vivo* patient measurements with an isotropic nominal resolution of 82 µm (Fig. 6). Given the larger voxel size, trabeculae may be reconstructed with a thickness of just one or two voxels. This necessitates the use of the so-called plate model to derive trabecular thickness (Tb.Th) and trabecular separation (Tb.Sp) from bone volume density and trabecular number (Tb.N), rather than using the direct 3D approach as implemented for higher resolution µCT. Nevertheless, the HR-pQCT morphometric measures correlate well to those of µCT (60). Furthermore, they provide excellent short-term and long-term reproducibility. At the distal radius, *in vivo* reproducibility of density was better than 0.59%, whereas for morphological measures this was better than <3.9% (61). Nevertheless, as with every CT, these systems require X-rays; hence, radiation dose, how little it may be, will always be a concern. With respect to these dose considerations, novel low-dose CT procedures and high-resolution magnetic resonance imaging (MRI) may have considerable potential for future clinical applications to overcome some of the limitations with the presented X-ray-based modalities (62;63).

Using HR-pQCT, three recent cross-sectional studies have shown sex- and age-related changes in trabecular structure and in cortical thickness of the distal radius *in vivo* (64-66). The acquired structural data were able to differentiate between osteopenic women with and without history of fracture, whereas measurements of BMD did not (64). Morphometric sex-specific differences in bone microstructure were found, potentially explaining the virtual absence of an age-related rise in distal

IBMS BoneKEy. 2008 November;5(11):410-425
http://www.bonekey-ibms.org/cgi/content/full/ibmske;5/11/410
doi: 10.1138/20080348

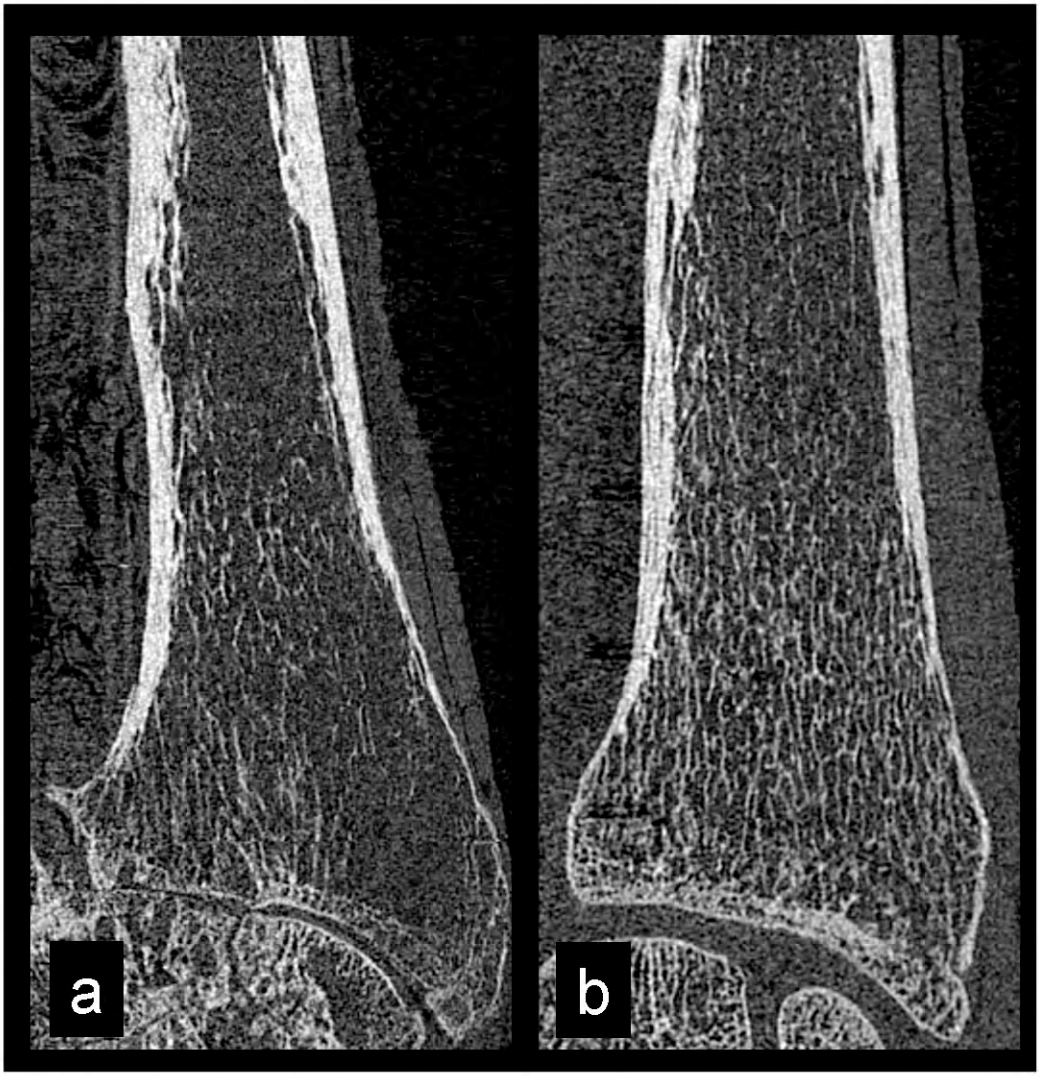

Fig. 6. High-resolution peripheral quantitative computed tomography (HR-pQCT) systems allow for the non-invasive measurement of human bone with resolution better than 100 µm. The figure shows HR-pQCT images, as measured *in vitro*, of the distal radius of a 79-year-old male (a) and a 92-year-old male (b), respectively (images courtesy of Thomas L. Mueller, ETH Zürich, Switzerland).

forearm fractures in men compared to the marked increase in these fractures in older women (66). In addition, relationships between hormonal and bone turnover variables and trabecular microstructure at the distal radius were demonstrated (65).

In combination with µFE analyses, these HR-pQCT data allow for the determination of bone competence *in vivo*. Ulrich *et al.* created µFE models to analyze an *in vivo* microarchitectural model of the distal radius, measured with an earlier pQCT providing lower resolution (67). This was the first time that tissue level stresses and strains were estimated in a living human subject. Pistoia *et al.* showed that there was good agreement between the predicted failure loads calculated from µFE and those measured using mechanical testing in a large sample of human cadaveric forearms. In addition, the µFE-derived strength parameters did substantially better in predicting experimental bone strength than classical bone densitometry (68). These data were confirmed for the newer version of

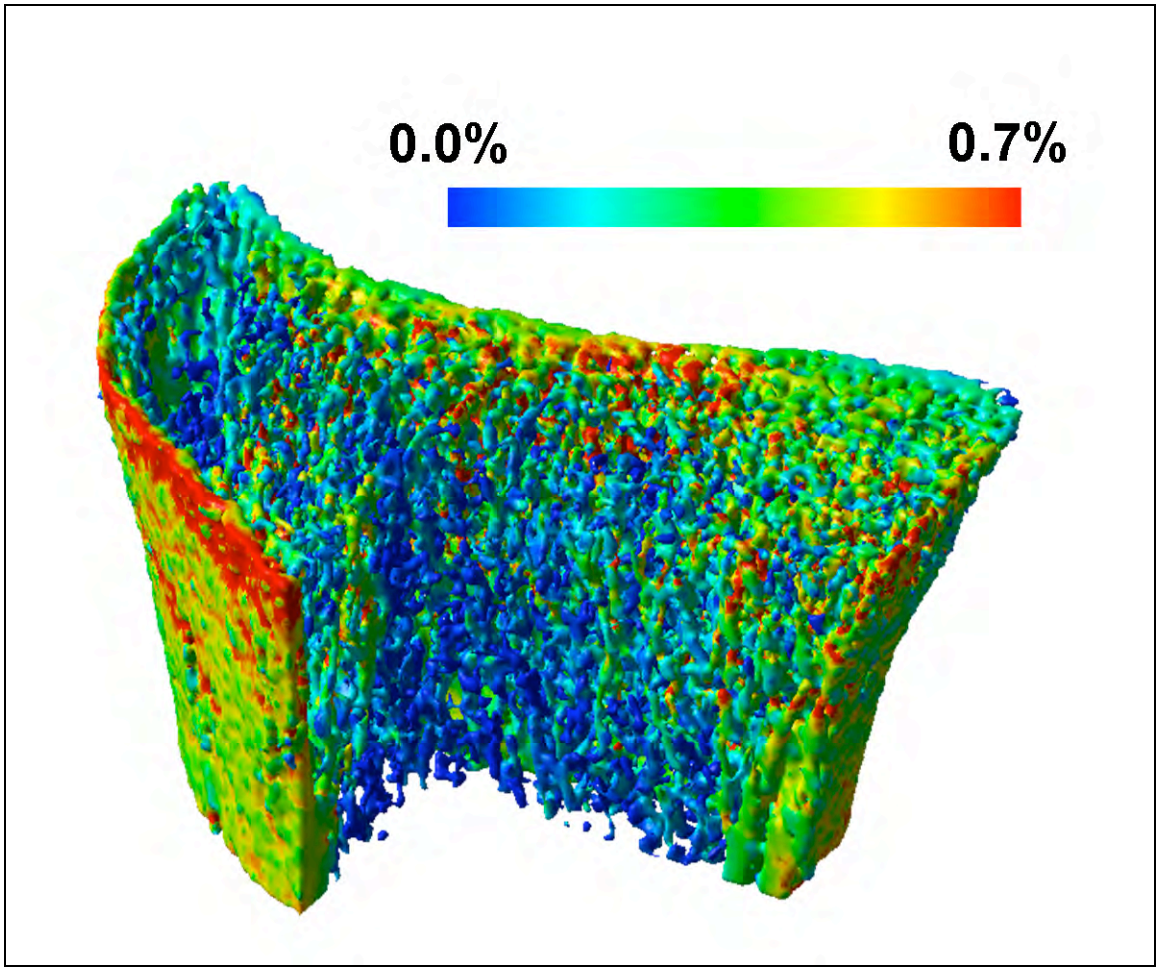

Fig. 7. The effective strain distribution in a 1 cm slab of bone from the distal radius as calculated from μFE analysis. The model was built from an *in vivo* high-resolution peripheral quantitative computed tomography (HR-pQCT) measurement; part of the bone was digitally removed to show the trabecular core.

the system that provides a nominal resolution of 82 μm (47). The potential of HR-pQCT-based μFE (Fig. 7) to identify people at risk of distal radius fracture has been demonstrated (69;70), indicating that it could become a clinical tool soon.

Conclusions

During the last decade microarchitectural bone imaging based on high-resolution CT has become the method of choice for quantifying 3D bone microstructure *in vitro*. It is a nondestructive, noninvasive, and precise procedure that allows the measurement of trabecular and compact bone, as well as the computation of microstructural and micromechanical properties. It has demonstrated its effectiveness in evaluating many applications such as the characterization of genetic effects in different mouse models and in quantifying microarchitectural changes resulting from diseases such as osteoporosis, the effects of hormones and medications such as estrogen and bisphosphonates, and effects of bone adaptation, such as those due to mechanical loading. Recent studies have shown the great potential of *in vivo* μCT for a better understanding of structural changes in bone geometry and its microstructure. These structural changes can be quantified using morphometric measures derived from the 3D data sets, and the effects on bone competence can be estimated from FE analyses. The ability to noninvasively track changes over time is likely to establish *in vivo* μCT as a standard methodology in the coming decade. The procedure might help

improve predictions of fracture risk, clarify the pathophysiology of skeletal diseases, and define the response to therapy. We expect these findings to improve our understanding of the influence of densitometric, morphological but also loading factors in the etiology of traumatic and spontaneous fractures of the forearm, the hip and the spine. Eventually, this improved understanding may lead to more successful approaches in the prevention of such age- and disease-related fractures.

Conflict of Interest: Dr. Müller reports that he is a founder and board member of b-cube AG. Dr. van Lenthe reports no conflict of interest.

Peer Review: This article has been peer-reviewed.

References

1. Keaveny TM, Pinilla TP, Crawford RP, Kopperdahl DL, Lou A. Systematic and random errors in compression testing of trabecular bone. *J Orthop Res*. 1997 Jan;15(1):101-10.

2. Carter DR, Hayes WC. The compressive behavior of bone as a two-phase porous structure. *J Bone Joint Surg Am*. 1977 Oct;59(7):954-62.

3. Rice JC, Cowin SC, Bowman JA. On the dependence of the elasticity and strength of cancellous bone on apparent density. *J Biomech*. 1988;21(2):155-68.

4. Wehrli FW, Saha PK, Gomberg BR, Song HK, Snyder PJ, Benito M, Wright A, Weening R. Role of magnetic resonance for assessing structure and function of trabecular bone. *Top Magn Reson Imaging*. 2002 Oct;13(5):335-55.

5. Turner CH, Cowin SC, Rho JY, Ashman RB, Rice JC. The fabric dependence of the orthotropic elastic constants of cancellous bone. *J Biomech*. 1990;23(6):549-61.

6. Van Rietbergen B, Odgaard A, Kabel J, Huiskes R. Relationships between bone morphology and bone elastic properties can be accurately quantified using high-resolution computer reconstructions. *J Orthop Res*. 1998 Jan;16(1):23-8.

7. Yang G, Kabel J, van Rietbergen B, Odgaard A, Huiskes R, Cowin SC. The anisotropic Hooke's law for cancellous bone and wood. *J Elast*. 1998-9;53(2):125-46.

8. Goulet RW, Goldstein SA, Ciarelli MJ, Kuhn JL, Brown MB, Feldkamp LA. The relationship between the structural and orthogonal compressive properties of trabecular bone. *J Biomech*. 1994 Apr;27(4):375-89.

9. Hodgskinson R, Currey JD. Separate effects of osteoporosis and density on the strength and stiffness of human cancellous bone. *Clin Biomech*. 1993 Sep;8(5):262-8.

10. Rincón-Kohli L, Zysset PK. Multi-axial mechanical properties of human trabecular bone. *Biomech Model Mechanobiol*. 2008 Aug 9; [Epub ahead of print]

11. Müller R, Hannan M, Smith SY, Bauss F. Intermittent ibandronate preserves bone quality and bone strength in the lumbar spine after 16 months of treatment in the ovariectomized cynomolgus monkey. *J Bone Miner Res*. 2004 Nov;19(11):1787-96.

12. Ritman EL. Micro-computed tomography-current status and developments. *Annu Rev Biomed Eng*. 2004;6:185-208.

13. Stauber M, Müller R. Micro-computed tomography: A method for the non-destructive evaluation of the three-dimensional structure of biological specimens. In: Westendorf JJ, ed. *Methods in Molecular Biology*. *Vol. 455: Osteoporosis: Methods and Protocols*. Totowa, NJ: Humana Press; 2008:273-92.

14. Müller R, Hildebrand T, Häuselmann HJ, Rüegsegger P. In vivo reproducibility of three-dimensional structural properties of noninvasive bone biopsies using 3D-pQCT. *J Bone Miner Res*. 1996 Nov;11(11):1745-50.

15. Balto K, Müller R, Carrington DC, Dobeck J, Stashenko P. Quantification of periapical bone destruction in mice by micro-computed tomography. *J Dent Res*. 2000 Jan;79(1):35-40.

16. Yamashita T, Nabeshima Y, Noda M. High-resolution micro-computed tomography analyses of the abnormal trabecular bone structures in klotho gene mutant mice. *J Endocrinol*. 2000 Feb;164(2):239-45.

17. Turner CH, Hsieh YF, Müller R, Bouxsein ML, Baylink DJ, Rosen CJ, Grynpas MD, Donahue LR, Beamer WG. Genetic regulation of cortical and trabecular bone strength and microstructure in inbred strains of mice. *J Bone Miner Res*. 2000 Jun;15(6):1126-31.

18. Alexander JM, Bab I, Fish S, Müller R, Uchiyama T, Gronowicz G, Nahounou M, Zhao Q, White DW, Chorev M, Gazit D, Rosenblatt M. Human parathyroid hormone 1-34 reverses bone loss in ovariectomized mice. *J Bone Miner Res*. 2001 Sep;16(9):1665-73.

19. Dempster DW, Cosman F, Kurland ES, Zhou H, Nieves J, Woelfert L, Shane E, Plavetic K, Müller R, Bilezikian J, Lindsay R. Effects of daily treatment with parathyroid hormone on bone microarchitecture and turnover in patients with osteoporosis: a paired biopsy study. *J Bone Miner Res*. 2001 Oct;16(10):1846-53.

20. Amling M, Herden S, Pösl M, Hahn M, Ritzel H, Delling G. Heterogeneity of the skeleton: comparison of the trabecular microarchitecture of the spine, the iliac crest, the femur, and the calcaneus. *J Bone Miner Res*. 1996 Jan;11(1):36-45.

21. Hildebrand T, Laib A, Müller R, Dequeker J, Rüegsegger P. Direct three-dimensional morphometric analysis of human cancellous bone: microstructural data from spine, femur, iliac crest, and calcaneus. *J Bone Miner Res*. 1999 Jul;14(7):1167-74.

22. Eckstein F, Matsuura M, Kuhn V, Priemel M, Müller R, Link TM, Lochmüller EM. Sex differences of human trabecular bone microstructure in aging are site-dependent. *J Bone Miner Res*. 2007 Jun;22(6):817-24.

23. Parfitt AM, Mathews CH, Villanueva AR, Kleerekoper M, Frame B, Rao DS. Relationships between surface, volume, and thickness of iliac trabecular bone in aging and in osteoporosis. Implications for the microanatomic and cellular mechanisms of bone loss. *J Clin Invest*. 1983 Oct;72(4):1396-409.

24. Odgaard A. Three-dimensional methods for quantification of cancellous bone architecture. *Bone*. 1997 Apr;20(4):315-28.

25. Stauber M, Müller R. Volumetric spatial decomposition of trabecular bone into rods and plates--a new method for local bone morphometry. *Bone*. 2006 Apr;38(4):475-84.

26. Stauber M, Rapillard L, van Lenthe GH, Zysset P, Müller R. Importance of individual rods and plates in the assessment of bone quality and their contribution to bone stiffness. *J Bone Miner Res*. 2006 Apr;21(4):586-95.

27. Liu XS, Sajda P, Saha PK, Wehrli FW, Bevill G, Keaveny TM, Guo XE. Complete volumetric decomposition of individual trabecular plates and rods and its morphological correlations with anisotropic elastic moduli in human trabecular bone. *J Bone Miner Res*. 2008 Feb;23(2):223-35.

28. Müller R, Gerber SC, Hayes WC. Micro-compression: a novel technique for the nondestructive assessment of local bone failure. *Technol Health Care*. 1998 Dec;6(5-6):433-44.

29. Nazarian A, Müller R. Time-lapsed microstructural imaging of bone failure behavior. *J Biomech*. 2004 Jan;37(1):55-65.

30. Nazarian A, Stauber M, Zurakowski D, Snyder BD, Müller R. The interaction of microstructure and volume fraction in predicting failure in cancellous bone. *Bone*. 2006 Dec;39(6):1196-202.

31. Müller R, Bösch T, Jarak D, Stauber M, Nazarian A, Tantillo M, Boyd SK. Micro-mechanical evaluation of bone microstructures under load. In: Bonse U, ed. *Developments in X-Ray Tomography III, Proceedings of SPIE 4503*. SPIE; 2002:189-200.

32. Verhulp E, van Rietbergen B, Huiskes R. A three-dimensional digital image correlation technique for strain measurements in microstructures. *J Biomech*. 2004 Sep;37(9):1313-20.

33. Zauel R, Yeni YN, Bay BK, Dong XN, Fyhrie DP. Comparison of the linear finite element prediction of deformation and strain of human cancellous bone to 3D digital volume correlation measurements. *J Biomech Eng*. 2006 Feb;128(1):1-6.

34. Christen D, Voide R, van Lenthe GH, Boyd SK, Müller R. Validation of a novel strain mapping algorithm based on deformable registration of µCT images. *J Biomech*. 2008 Jul;41(Suppl 1):S122.

35. Keaveny TM, Morgan EF, Niebur GL, Yeh OC. Biomechanics of trabecular bone. *Annu Rev Biomed Eng*. 2001;3:307-33.

36. Ladd AJ, Kinney JH, Haupt DL, Goldstein SA. Finite-element modeling of trabecular bone: comparison with mechanical testing and determination of tissue modulus. *J Orthop Res*. 1998 Sep;16(5):622-8.

37. Kabel J, van Rietbergen B, Dalstra M, Odgaard A, Huiskes R. The role of an effective isotropic tissue modulus in the elastic properties of cancellous bone. *J Biomech*. 1999 Jul;32(7):673-80.

38. Homminga J, McCreadie BR, Weinans H, Huiskes R. The dependence of the elastic properties of osteoporotic cancellous bone on volume fraction and fabric. *J Biomech*. 2003 Oct;36(10):1461-7.

39. Niebur GL, Feldstein MJ, Yuen JC, Chen TJ, Keaveny TM. High-resolution finite element models with tissue strength asymmetry accurately predict failure of trabecular bone. *J Biomech*. 2000 Dec;33(12):1575-83.

40. Bayraktar HH, Morgan EF, Niebur GL, Morris GE, Wong EK, Keaveny TM. Comparison of the elastic and yield properties of human femoral trabecular and cortical bone tissue. *J Biomech*. 2004 Jan;37(1):27-35.

41. van Rietbergen B, Huiskes R, Eckstein F, Rüegsegger P. Trabecular bone tissue strains in the healthy and osteoporotic human femur. *J Bone Miner Res*. 2003 Oct;18(10):1781-8.

42. Homminga J, Van Rietbergen B, Lochmüller EM, Weinans H, Eckstein F, Huiskes R. The osteoporotic vertebral structure is well adapted to the loads of daily life, but not to infrequent "error" loads. *Bone*. 2004 Mar;34(3):510-6.

43. Eswaran SK, Gupta A, Adams MF, Keaveny TM. Cortical and trabecular load sharing in the human vertebral body. *J Bone Miner Res*. 2006 Feb;21(2):307-14.

44. Arbenz P, van Lenthe GH, Mennel U, Müller R, Sala M. A scalable multi-level preconditioner for matrix-free µ-finite element analysis of human bone structures. *Int J Numer Methods Eng*. 2008 Feb 12;73(7):927-47.

45. Arbenz P, van Lenthe GH, Müller R, Wirth AJ, Bekas C, Curioni A. Extreme scalability challenges in analyses of human bone structures. Joint Meeting of the 8th World Congress on Computational Mechanics (WCCM8) and 5th European Congress on Computational Methods in Applied Sciences and Engineering (ECCOMAS 2008), Venice, Italy, June 30 - July 5, CD-ROM; 2008.

46. Mueller TL, Stauber M, Kohler T, Eckstein F, Müller R, van Lenthe GH. Non-invasive bone competence analysis by high-resolution pQCT: An in vitro reproducibility study on structural and mechanical properties at the human radius. *Bone*. 2008 Nov 3; [Epub ahead of print]

47. Macneil JA, Boyd SK. Bone strength at the distal radius can be estimated from high-resolution peripheral quantitative computed tomography and the finite element method. *Bone*. 2008 Jun;42(6):1203-13.

48. Kinney JH, Lane NE, Haupt DL. In vivo, three-dimensional microscopy of trabecular bone. *J Bone Miner Res*. 1995 Feb;10(2):264-70.

49. Lane NE, Thompson JM, Haupt D, Kimmel DB, Modin G, Kinney JH. Acute changes in trabecular bone connectivity and osteoclast activity in the ovariectomized rat in vivo. *J Bone Miner Res*. 1998 Feb;13(2):229-36.

50. David V, Laroche N, Boudignon B, Lafage-Proust MH, Alexandre C, Rüegsegger P, Vico L. Noninvasive in vivo monitoring of bone architecture alterations in hindlimb-unloaded female rats using novel three-dimensional microcomputed tomography. *J Bone Miner Res*. 2003 Sep;18(9):1622-31.

51. Waarsing JH, Day JS, van der Linden JC, Ederveen AG, Spanjers C, De Clerck N, Sasov A, Verhaar JA, Weinans H. Detecting and tracking local changes in the tibiae of individual rats: a novel method to analyse longitudinal in vivo micro-CT data. *Bone*. 2004 Jan;34(1):163-9.

52. Kohler T, Beyeler M, Webster D, Müller R. Compartmental bone morphometry in the mouse femur: reproducibility and resolution dependence of microtomographic measurements. *Calcif Tissue Int*. 2005 Nov;77(5):281-90.

53. Brouwers JE, van Rietbergen B, Huiskes R. No effects of in vivo micro-CT radiation on structural parameters and bone marrow cells in proximal tibia of wistar rats detected after eight weekly scans. *J Orthop Res*. 2007 Oct;25(10):1325-32.

54. Klinck RJ, Campbell GM, Boyd SK. Radiation effects on bone architecture in mice and rats resulting from in vivo micro-computed tomography scanning. *Med Eng Phys*. 2008 Sep;30(7):888-95.

55. Waarsing JH, Day JS, Verhaar JA, Ederveen AG, Weinans H. Bone loss dynamics result in trabecular alignment in aging and ovariectomized rats. *J Orthop Res*. 2006 May;24(5):926-35.

56. Boyd SK, Davison P, Müller R, Gasser JA. Monitoring individual morphological changes over time in ovariectomized rats by in vivo micro-computed tomography. *Bone*. 2006 Oct;39(4):854-62.

57. Brouwers JE, Lambers FM, Gasser JA, van Rietbergen B, Huiskes R. Bone degeneration and recovery after early and late bisphosphonate treatment of ovariectomized wistar rats assessed by in vivo micro-computed tomography. *Calcif Tissue Int*. 2008 Mar;82(3):202-11.

58. Klinck J, Boyd SK. The magnitude and rate of bone loss in ovariectomized mice differs among inbred strains as determined by longitudinal in vivo micro-computed tomography. *Calcif Tissue Int*. 2008 Jul;83(1):70-9.

59. Borah B, Dufresne TE, Chmielewski PA, Johnson TD, Chines A, Manhart MD. Risedronate preserves bone architecture in postmenopausal women with osteoporosis as measured by three-dimensional microcomputed tomography. *Bone*. 2004 Apr;34(4):736-46.

60. MacNeil JA, Boyd SK. Accuracy of high-resolution peripheral quantitative computed tomography for measurement of bone quality. *Med Eng Phys*. 2007 Dec;29(10):1096-1105.

61. MacNeil JA, Boyd SK. Improved reproducibility of high-resolution peripheral quantitative computed tomography for measurement of bone quality. *Med Eng Phys*. 2008 Jul;30(6):792-9.

62. Kazakia GJ, Majumdar S. New imaging technologies in the diagnosis of osteoporosis. *Rev Endocr Metab Disord*. 2006 Jun;7(1-2):67-74.

63. Bouxsein ML. Technology insight: noninvasive assessment of bone strength in osteoporosis. *Nat Clin Pract Rheumatol*. 2008 Jun;4(6):310-8.

64. Boutroy S, Bouxsein ML, Munoz F, Delmas PD. In vivo assessment of trabecular bone microarchitecture by high-resolution peripheral quantitative computed tomography. *J Clin Endocrinol Metab*. 2005 Dec;90(12):6508-15.

65. Khosla S, Melton LJ 3rd, Achenbach SJ, Oberg AL, Riggs BL. Hormonal and biochemical determinants of trabecular microstructure at the ultradistal radius in women and men. *J Clin Endocrinol Metab*. 2006 Mar;91(3):885-91.

66. Khosla S, Riggs BL, Atkinson EJ, Oberg AL, McDaniel LJ, Holets M, Peterson JM, Melton LJ 3rd. Effects of sex and age on bone microstructure at the ultradistal radius: a population-based noninvasive in vivo assessment. *J Bone Miner Res*. 2006 Jan;21(1):124-31.

67. Ulrich D, van Rietbergen B, Laib A, Rüegsegger P. Load transfer analysis of the distal radius from in-vivo high-resolution CT-imaging. *J Biomech*. 1999 Aug;32(8):821-8.

68. Pistoia W, van Rietbergen B, Lochmüller EM, Lill CA, Eckstein F, Rüegsegger P. Estimation of distal radius failure load with micro-finite element analysis models based on three-dimensional peripheral quantitative computed tomography images. *Bone*. 2002 Jun;30(6):842-8.

69. Melton LJ 3rd, Riggs BL, van Lenthe GH, Achenbach SJ, Müller R, Bouxsein ML, Amin S, Atkinson EJ, Khosla S. Contribution of in vivo structural measurements and load/strength ratios to the determination of forearm fracture risk in postmenopausal women. *J Bone Miner Res*. 2007 Sep;22(9):1442-8.

70. Boutroy S, Van Rietbergen B, Sornay-Rendu E, Munoz F, Bouxsein ML, Delmas PD. Finite element analysis based on in vivo HR-pQCT images of the distal radius is associated with wrist fracture in postmenopausal women. *J Bone Miner Res*. 2008 Mar;23(3):392-9.